# Nucleotide-Dependent Movements of the Kinesin Motor Domain Predicted by Simulated Annealing

Willy Wriggers and Klaus Schulten
Department of Physics and Beckman Institute, University of Illinois at Urbana-Champaign, Urbana, Illinois 61801 USA

ABSTRACT The structure of an ATP-bound kinesin motor domain is predicted and conformational differences relative to the known ADP-bound form of the protein are identified. The differences should be attributed to force-producing ATP hydrolysis. Candidate ATP-kinesin structures were obtained by *simulated annealing*, by placement of the ATP $\gamma$-phosphate in the crystal structure of ADP-kinesin, and by interatomic distance constraints. The choice of such constraints was based on mutagenesis experiments, which identified Gly-234 as one of the $\gamma$-phosphate sensing residues, as well as on structural comparison of kinesin with the homologous nonclaret disjunctional (ncd) motor and with G-proteins. The prediction of nucleotide-dependent conformational differences reveals an allosteric coupling between the nucleotide pocket and the microtubule binding site of kinesin. Interactions of ATP with Gly-234 and Ser-202 trigger structural changes in the motor domain, the nucleotide acting as an allosteric modifier of kinesin's microtubule-binding state. We suggest that in the presence of ATP kinesin's putative microtubule binding regions L8, L12, L11, $\alpha$4, $\alpha$5, and $\alpha$6 form a face complementary in shape to the microtubule surface; in the presence of ADP, the microtubule binding face adopts a more convex shape relative to the ATP-bound form, reducing kinesin's affinity to the microtubule.

## INTRODUCTION

Kinesin is the founding member of a superfamily of microtubule-based motor proteins that perform force-generating tasks such as organelle transport and chromosome segregation (Barton and Goldstein, 1996; Hirokawa, 1996). The motor can move along more than 100 tubulin subunits before dissociating from the microtubule track (Howard et al., 1989). Kinesin advances in 8-nm increments, corresponding to the spacing between $\alpha/\beta$ tubulin subunits on the microtubule protofilament (Svoboda et al., 1993). The metabolic energy that drives kinesins and the larger myosin and dynein motor proteins is provided in the form of ATP (Hackney, 1996). The energy released by ATP hydrolysis is converted into directed movement after kinesin binds strongly to the microtubule (Howard, 1996; Ma and Taylor, 1997). Recently, the crystal structures of two members of the kinesin superfamily, conventional kinesin (Kull et al., 1996) and the kinesin-related *ncd* gene (nonclaret disjunctional) product from *Drosophila*, ncd (Sablin et al., 1996), were reported. The discovery led to unexpected insights into structural homologies and possible evolutionary relationships between kinesins and G-proteins (Vale, 1996) and between kinesins and myosin motor proteins (Rayment, 1996; Hackney, 1996; Sellers, 1996). The small size ($\approx$340 aa) of the kinesin motor domain renders the enzyme suitable for an investigation of the structural mechanisms that are fundamental to ATP-driven motility. This paper is concerned with the mechanism of kinesin's $\gamma$-phosphate recognition and the conformational response to ATP-hydrolysis.

Fig. 1 compares the crystal structures of the ncd and kinesin motor or head domains superimposed by their common $Mg^{2+}$-ADP nucleotide. The arrowhead-shaped structures (41% sequence identity) are highly homologous. The core structural elements of the head domains (146 $\alpha$-carbons) including a central eight-stranded $\beta$-sheet can be superimposed with an rms deviation of 1.2 Å (Sablin et al., 1996). Kinesin and ncd are dimeric proteins that are each composed of two heads held together by an $\alpha$-helical coiled coil neck region (Stewart et al., 1993; Morii et al., 1997) which is missing in the crystal structures. The polypeptides differ in their functional properties and in their composition: kinesin is a microtubule plus-end directed motor (Vale et al., 1985) which has its head attached at the N-terminus of the protein chain (Yang et al., 1990); ncd moves toward the microtubule minus-end (McDonald et al., 1990; Walker et al., 1990) and has its head at the C-terminus of the chain (McDonald and Goldstein, 1990). Kinesin and ncd exhibit similar kinetic properties (Lockhart and Cross, 1994; Shimizu et al., 1995; Lockhart et al., 1995; Crevel et al., 1996) as well as the same binding geometry of a single head relative to the microtubule (Hoenger and Milligan, 1997; Hirose et al., 1997). The reversal in the direction of movement observed in an ncd-kinesin chimera indicates that the directionality is not an exclusive property of the motor domain (Henningsen and Schliwa, 1997). Differences in motor directionality probably arise from specific interactions between the heads in the dimer. When one head is bound to the microtubule, the second, unattached head is oriented toward the microtubule plus-end in the case of

*Received for publication 10 November 1997 and in final form 8 January 1998.*

Address reprint requests to Dr. Klaus Schulten, Department of Physics, Beckman Institute 3147, University of Illinois, 405 N. Mathews Ave., Urbana, IL 61801. Tel.: 217-244-1604; Fax: 217-244-6078; E-mail: kschulte@ks.uiuc.edu.

Dr. Wriggers' current address is Department of Chemistry & Biochemistry, University of California, San Diego, La Jolla, CA 92093-0365.



0006-3495/98/08/646/16 $2.00

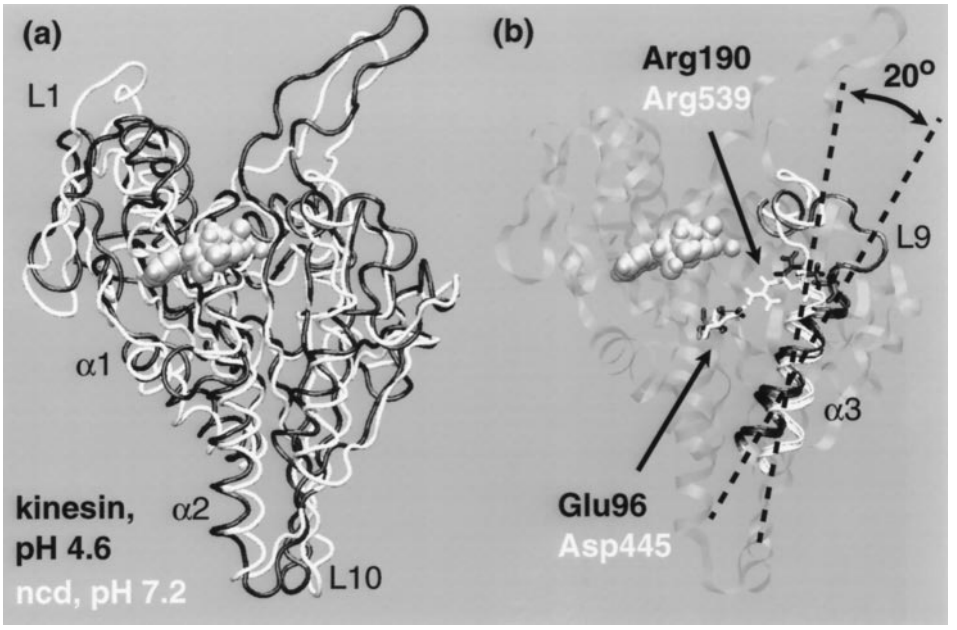


FIGURE 1 Comparison of kinesin (Kull et al., 1996; black) and ncd (Sablin et al., 1996; white) crystal structures (front view). (*a*) Kinesin and ncd, in tube-representation, are compared by superimposing the common $Mg^{2+}$-ADP complex (gray van der Waals representation). Structure elements (Kull et al., 1996) discussed in the text are indicated. (*b*) A putative pH-dependent salt bridge involving conserved residues stabilizes the orientation of helix $\alpha$3. The figure was generated with the molecular graphics program *VMD* (Humphrey et al., 1996).

kinesin, and toward the minus-end in the case of ncd (Hirose et al., 1996; Arnal et al., 1996).

Recently, a model of ncd bound to a microtubule emerged from low-resolution electron microscopy data (Sosa et al., 1997). The identified microtubule-binding face of ncd corresponds to kinesin's structural elements L8, L11, L12, $\alpha$4, and $\alpha$6, which are presented in Fig. 2. Alanine scanning mutagenesis (Woehlke et al., 1997) suggested that the core of the microtubule-binding face is formed by loop L12 and the adjacent helix $\alpha$5. This small region (Fig. 2) is believed to contribute the majority of the binding free energy in the complex. Kinesin and ncd share similar mechanisms of attachment to the microtubule. For a kinesin or ncd motor to move along the microtubule, both tightly bound and detachable states are required (Crevel et al., 1996). Tightly bound states sustain force and dissociate slowly under tension, whereas detachable states bind weakly and dissociate rapidly from the microtubule track, thereby making possible the movement of the motor. In the present work we investigate how nucleotide-dependent changes in the enzymatic site can modify the conformation of the distant microtubule binding site and how the nucleotide hydrolysis cycle is coupled to the strength of binding of the motor to its track.

Minor differences between the structures of kinesin and ncd can be found in their surface loops and in two helices (Sablin et al., 1996). The most variable helix, termed $\alpha$3, exhibits a change in orientation by 20° (Fig. 1 *b*). This helix is loosely packed (51% of its surface is solvent-accessible) and its reorientation may be due to the different pH conditions under which ncd and kinesin were crystallized. In ncd, at pH 7.2 (Sablin and Fletterick, 1995), Asp-445 forms a salt bridge with Arg-539. The expected $pK_a$ of the corresponding acidic residue Glu-96 in kinesin is 4.4–4.6 (Cantor and Schimmel, 1980). At pH 4.6 (Kull et al., 1996), kinesin's Glu-96 is considerably more protonated than ncd's Asp-445 at pH 7.2. It is possible that the lower pH in kinesin severs the salt bridge with the corresponding Arg-190. The absence of the salt bridge appears to facilitate the mentioned rotation of the loosely packed helix presented in Fig. 1 *b*. The arginine residue involved in this putative pH-dependent salt bridge is absolutely conserved among kinesin sequences (Sablin et al., 1996) and is located in close proximity to the nucleotide, raising the question whether Arg-190 is involved in kinesin's enzymatic mechanism. In this work we tested whether at neutral pH Glu-96 may form a salt bridge with Arg-190, and whether differences in the behavior of helix $\alpha$3 can be attributed to the type of bound nucleotide, ATP or ADP.

Unfortunately, researchers have not been able so far to crystallize kinesin in complex with a nonhydrolyzable ATP-analog which would reveal, by comparison with the ADP-kinesin crystal structure (Kull et al., 1996), the structural mechanism of the force-producing ATP hydrolysis. The surprising homology of the kinesin nucleotide binding region with corresponding regions in myosin and G-proteins, however, led to a plausible model of nucleotide-dependent changes induced in the kinesin structure in the presence of the additional $\gamma$-phosphate of ATP (Vale, 1996). According to this model, two "switch" loops contact the $\gamma$-phosphate and amplify conformational changes through movement of nearby structural elements. Two residues in particular were identified as putative $\gamma$-phosphate sensors: Ser-202 in the switch I loop, corresponding to the $\gamma$-phosphate sensor Ser-243 in chicken myosin and Thr-35 in p21 ras G-proteins, and Gly-234 in the switch II loop, corresponding to the $\gamma$-phosphate sensor Gly-466 in chicken myosin and Gly-60 in p21 ras G-proteins (Kull et al., 1996; Sablin et al., 1996). Alanine substitutions of these residues in kinesin yielded completely inactive motors (R. D. Vale, personal

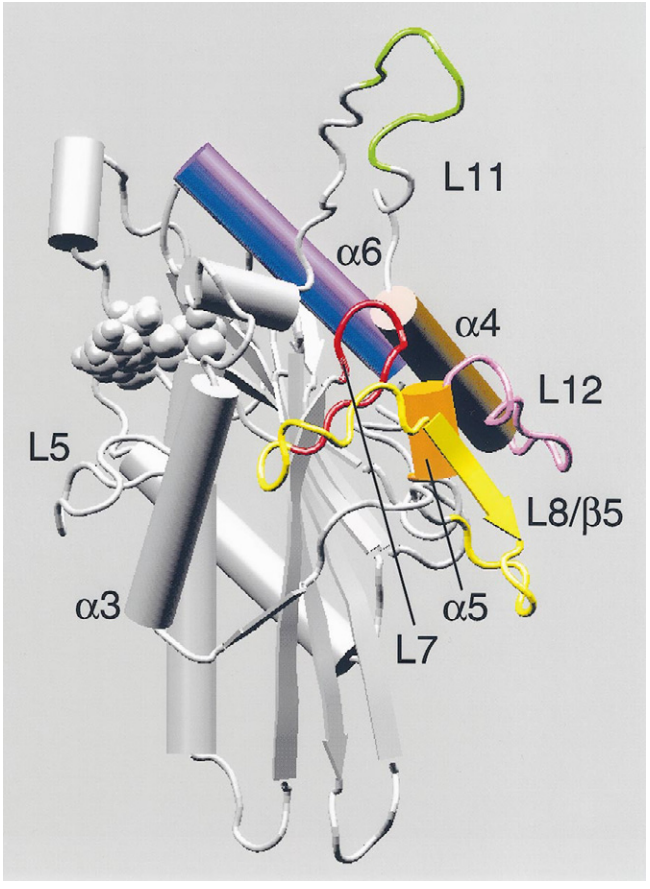


FIGURE 2 Microtubule-binding regions in kinesin. The protein is rotated by 90° relative to the orientation in Fig. 1. Kinesin (Kull et al., 1996) is shown in cartoon representation. $Mg^{2+}$-ADP is shown in van der Waals representation. A sequence of conserved residues among kinesin family members (Sablin et al., 1996), ExYx(E/D)xxxDLL, is shown in red (loop L7, 136–148). This fingerprint forms the basis of an exposed loop/sheet region (L8/β5, 149–163, yellow) which binds to β-tubulin (Sosa et al., 1997). A second conserved fingerprint, (I/V)P(F/Y)R is part of the exposed MT-binding loop L12 (271–280, purple), which is believed to interact strongly with the microtubule (Sosa et al., 1997; Woehlke et al., 1997). Other putative MT-regions, as identified by Sosa et al., 1997; Woehlke et al., 1997 are helix α4 (256–270, brown), helix α5 (281–290, orange), the tip of loop L11 (243–250, green), and helix α6 (306–321, blue). The figure was generated with the molecular graphics program *VMD* (Humphrey et al., 1996).

communication), confirming a critical role of these residues in the mechanochemical cycle.

To predict the structure of ATP-kinesin and to test whether the nucleotide-dependent changes predicted by the switch I/II model arise in this structure, we adopted a computational procedure that enforced geometric constraints based on mutagenesis data and on structural homology. The procedure combines distance constraints with a conformational search technique, *simulated annealing* (van Laarhoven and Aarts, 1987; Brünger et al., 1990; Brünger, 1991). This search technique allows proteins to cross barriers between local minima in the hierarchical protein energy surface (Frauenfelder et al., 1991; Huber and McCammon, 1997) faster than would be possible by simulations at room temperature. Simulated annealing thereby accelerates the relaxation of the system from any imposed constraints or from unfavorable interactions. The computational cost of an exhaustive search for global energy minima by simulated annealing is prohibitively high (Huber and McCammon, 1997). Therefore, we have biased the conformational search by distance constraints that induce minimal, knowledge-based perturbations to the crystal structure of ADP-kinesin.

## METHODS

### Placement of γ-phosphate

We modeled ATP-kinesin starting from the ADP-crystal structure (Kull et al., 1996). Missing parts of the crystal structure (the N-terminus and part of the disordered loop L11) were added by F. Jon Kull (personal communication). When ADP is exchanged for ATP, the protein has to provide additional ligands to stabilize the γ-phosphate. The coordination of the nucleotide is best understood for G-proteins, where the nucleotide binding pocket was found in a more open conformation in the GDP state compared to the GTP state (Mixon et al., 1995; Lambright et al., 1994; Milburn et al., 1990). We assumed that in kinesin the γ-phosphate arising under replacement of ADP by ATP in the nucleotide-binding site will not be obstructed by residues of ADP-kinesin. A model of ATP-kinesin must also account for the interactions between the nucleotide and an $Mg^{2+}$-ion expected to be associated with ADP or ATP in kinesin. This ion is coordinated by the β- and γ-phosphates in G-proteins (Pai et al., 1989; Noel et al., 1993; Mixon et al., 1995; Lambright et al., 1994; Milburn et al., 1990; Berchtold et al., 1993) and in ATPases such as actin (Kabsch et al., 1990) and myosin (Fisher et al., 1995; Smith and Rayment, 1996). There are three β-oxygens of ADP that could form phosphoester bonds with the γ-phosphate of ATP. In addition, for each such bond there exist three intrinsically stable conformations characterized through different dihedral angles $O_\alpha$-$P_\beta$-$O_\beta$-$P_\gamma$. We superimposed the ATP β- and γ-phosphates from a crystal structure of the protein actin (Kabsch et al., 1990) with the β-phosphate of ADP-kinesin in the nine possible combinations of β-oxygen and dihedral angle $O_\alpha$-$P_\beta$-$O_\beta$-$P_\gamma$. We then chose the ATP conformation that exhibited the fewest steric clashes with the protein and properly coordinated the $Mg^{2+}$-ion; of the nine possible combinations of β-oxygen and corresponding dihedral angle, a single conformation emerged clearly as most favorable in this respect. After construction, the nucleotide was energy-minimized.

### Placement of water molecules

Bound water is known to play an important functional role in proteins (Westhof, 1993). Water molecules that are trapped inside a protein often stabilize its conformation and can be considered an integral part of the protein's structure (Ernst et al., 1995). Unfortunately, due to their positional disorder, water molecules are, in many cases, not well resolved by x-ray crystallography. Hence, for a realistic simulation of a protein, empty cavities in crystal structures need to be filled by water molecules. We predicted, based on energetic considerations, the position of buried water molecules in kinesin with the program *Dowser* (Zhang and Hermans, 1996), using default energetic parameters. Fig. 3 shows the predicted water molecules together with water molecules observed in the crystal structure (Kull et al., 1996). *Dowser*-placed water molecules confirm the position of seven buried crystallographic water molecules and predict six additional water binding sites. We included these six predicted water molecules, together with the crystal water molecules, in our model.

To account for the effect of surface water, the system was immersed in a shell of explicit water molecules of 10 Å thickness, which corresponds to approximately four layers of water molecules (Fig. 3). The water shell was constructed by covering the outside of the system with a three-dimensional lattice of water cubes provided by X-PLOR (Brünger, 1992). The cubes of 15.55 $Å^3$ size each contained 125 water molecules, resulting in uniformly

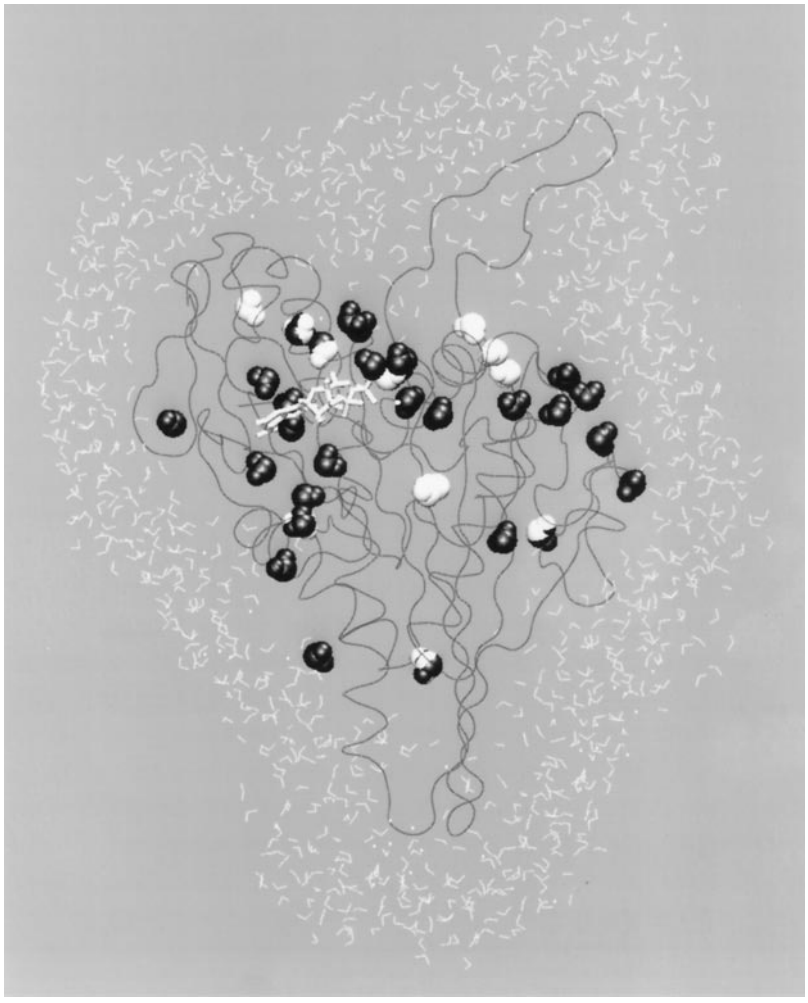

FIGURE 3 Placement of buried and solvent water molecules. Twenty-nine crystal water molecules (Kull et al., 1996) are shown in black van der Waals representation. The protein is represented by a backbone trace. The nucleotide is rendered in licorice style. We predicted the position of buried water molecules with the program *Dowser* (Zhang and Hermans, 1996). The predicted water molecules are shown in white van der Waals representation. Seven of the crystal water molecules are buried. The positions of these water molecules were confirmed by *Dowser*. In addition, *Dowser* found six empty cavities in the protein structure, which are likely occupied by water molecules (some water molecules are obstructed from view). Also shown (in white line representation) are selected water molecules surrounding the protein that represent the solvent shell included in the present simulations. The figure was generated with the molecular graphics program *VMD* (Humphrey et al., 1996).

distributed water of density 1.0 g $cm^{-3}$ $H_2O$. After solvation, the total size of ADP-kinesin was 15,599 atoms, and the total size of ATP-kinesin was 15,603 atoms. The two systems each contained 3489 water molecules.

## Structural refinement

The kinesin structures were refined by simulated annealing simulation protocols, using a maximum annealing temperature of 500 K. After an initial energy-minimization, the systems were assigned initial velocities according to a Maxwell distribution and heated up to 500 K in steps of 10 K by Langevin dynamics (Pastor, 1994; Brünger, 1992) over a 50-ps time period, using a uniform friction constant $\beta = 50$ $ps^{-1}$ for heavy atoms and $\beta = 0$ for hydrogens. The systems were then cooled down from 500 K in steps of 2.5 K over a 120-ps time period (Fig. 4). The annealing was stopped at the low temperature of 200 K, which quenched the mobility of the cooled system. The final structures were energy-minimized after a total of 170 ps of simulation.

The simulations described in this paper were carried out with the program X-PLOR (Brünger, 1992). A dielectric constant $\epsilon = 1$, an integration time step of 1 fs, and a cutoff distance of 12 Å for nonbonded interactions were chosen. The parameters of the CHARMM all-atom force field (Brooks et al., 1983), version 22, were used to account for the interactions of protein, $Mg^{2+}$, and water atoms. The interactions of the ADP and ATP nucleotides were described, in certain cases (specified below), by the force field developed by us (Wriggers and Schulten, 1997b), and in other cases by the CHARMM force field (Brooks et al., 1983), version 24. The TIP3(P) water model (Jorgensen et al., 1983) was modified by omitting the H–H bond and internal geometry constraints to provide water flexibility. This modification was motivated by molecular dynamics (MD) studies, which demonstrate an improvement of physical properties of flexible water over the rigid TIP3 model (Teeter, 1991; Daggett and Levitt, 1993). Flexible TIP3P water also exhibits values for the water density, heat of vaporization, and diffusion coefficient as close to the experimental values as those obtained with the original TIP3P model (Steinbach and Brooks, 1993; Guàrdia and Padró, 1996).

## Distance constraints

We employed distance constraints in certain simulated systems to induce desired conformational transitions. Recently, a related technique involving geometric constraints, termed *activated molecular dynamics*, was successfully applied to induce flap opening events in HIV-1 protease (Collins et al., 1995). We enforced the proper coordination of the $\gamma$-phosphate in ATP-kinesin by constraining the distance between the $\gamma$-phosphate and Gly-234. The distance between the $\gamma$-phosphorus and the $\alpha$-carbon of Gly-234 was constrained by a Hookean potential to 3.9 Å (distance derived from the geometry of $\beta$-coordinating residues). We varied the force constant used to constrain the atoms (1.0 and 5.0 kcal $mol^{-1}$ $Å^{-2}$). To test the hypothesis that in kinesin Glu-96 forms a salt bridge with Arg-190 at neutral pH (Fig. 1), we induced the formation of the salt bridge by a distance constraint between atom HH22 of Arg-190 and Glu-96. To avoid favoring one acidic oxygen of Glu-96 over the other, the carbon CD atom was chosen as a constraint point. The minimum of the Hookean potential

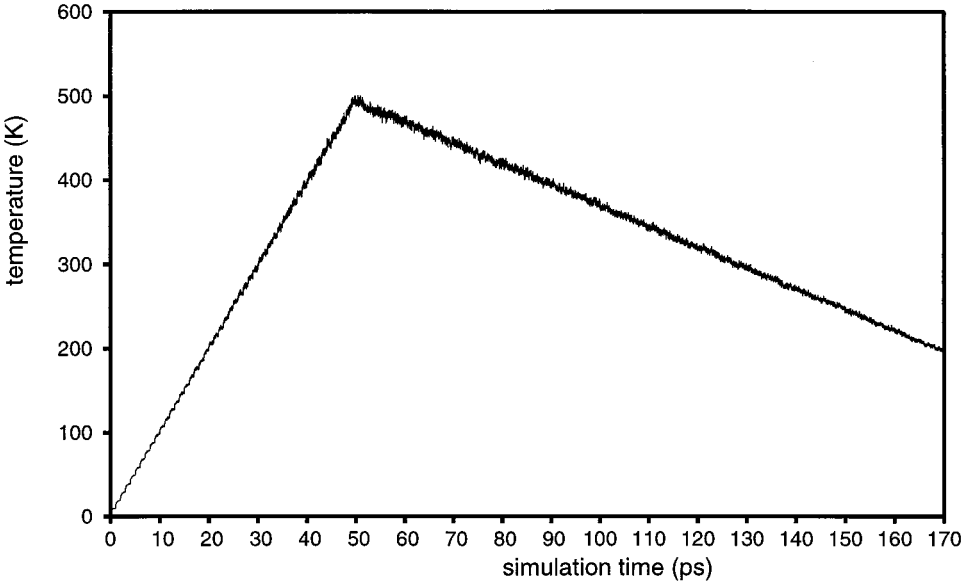


FIGURE 4 The temperature as a function of simulation time during the refinement of structure ST (Table 1).

was at a distance of 2.4 Å, derived from the distance between Asp-445 and Arg-539 in the crystal structure of ncd (Sablin et al., 1996).

An overview of the annealing runs is given in Table 1. [The resulting structures are available via anonymous ftp at ftp://ftp.ks.uiuc.edu/ in directory /pub/projects/kinesin/structures.] A first, exploratory series of annealing runs in the absence of distance constraints involved ADP-kinesin, ATP-kinesin, and nucleotide-free kinesin. The resulting structures will be referred to as SD, ST, and SF, respectively. The SF structure served to evaluate the stability of the enzymatic site, which remained stable in the absence of the nucleotide. In a second round of annealing runs, ADP-kinesin was again unconstrained, but in this case the run started with a set of random initial velocities different from the one used in the refinement of structure SD. ATP-kinesin was simulated with a weak (1.0 kcal $mol^{-1}$ $Å^{-2}$) constraint between the γ-phosphate and Gly-234. The two resulting structures are termed AD and AT, respectively. A third series of annealing runs was carried out with a strong (5.0 kcal $mol^{-1}$ $Å^{-2}$) constraint of the Glu-96–Arg-190 distance in ADP-kinesin, and a strong constraint of the distance between the γ-phosphate and Gly-234. The corresponding structures are termed BD and BT. In a fourth round of annealing runs of unconstrained ADP-kinesin and of ATP-kinesin with a strong constraint between the γ-phosphate and Gly-234, we altered the mentioned nucleotide force fields (Wriggers and Schulten, 1997b; Brooks et al., 1983) to verify the independence of the behavior of the nucleotide conformation on the choice of the specific force field (Table 1). The resulting structures will be referred to as CD and CT. Finally, a fifth series of annealing runs involved a strong constraint of the Glu-96–Arg-190 distance in ADP-kinesin and strong constraints of the distances Glu-96–Arg-190 and γ-phosphate–Gly-234 in ATP-kinesin. The corresponding structures are termed DD and DT, respectively.

## Analysis of structures

### *Fluctuations*

Root-mean-square fluctuations $\rho_i$ exhibited by atoms $i$ in a set of least-squares fitted (Kabsch, 1976) structures $k = 1, 2, \cdots, N$ were computed according to

$$\rho_i^2 = \langle \Delta r_i^2 \rangle = \frac{1}{N} \sum_{k=1}^{N} \Delta r_i^2, \quad (1)$$

where $\Delta r_i$ is the atomic displacement of atom $i$ from its average position in the $N$ structures chosen. The fluctuations were then averaged over the atoms of a residue and plotted as a function of residue number. Crystal

**TABLE 1 Overview of simulated structures**

| | | Constraints (kcal $mol^{-1}$ $Å^{-2}$) | | |
|---|---|---|---|---|
| Structure | Nucleotide | γ-Gly-234 | Glu-96–Arg-190 | Nucleotide Force Field |
| SD | ADP | — | — | Wriggers and Schulten |
| ST | ATP | — | — | Wriggers and Schulten |
| SF | — | — | — | — |
| AD | ADP | — | — | Wriggers and Schulten |
| AT | ATP | 1.0 | — | Wriggers and Schulten |
| BD | ADP | — | 5.0 | Wriggers and Schulten |
| BT | ATP | 5.0 | — | Wriggers and Schulten |
| CD | ADP | — | — | CHARMM, version 24 |
| CT | ATP | 5.0 | — | CHARMM, version 24 |
| DD | ADP | — | 5.0 | CHARMM, version 24 |
| DT | ATP | 5.0 | 5.0 | CHARMM, version 24 |

The nucleotide force fields used include Wriggers and Schulten, 1997b, and the CHARMM force field (Brooks et al., 1983), version 24.

*B*-factors (R. J. Fletterick, personal communication) were compared with the atomic fluctuations using the relationship

$$\langle \Delta r_i^2 \rangle_C = 3B_i/(8\pi^2), \quad (2)$$

where $B_i$ is the *B*-factor corresponding to atom *i* and $\langle \cdots \rangle_C$ denotes the spatiotemporal average of squared displacements $\Delta r_i$ in the crystal. The square root of the rhs in Eq. 2 was averaged over the atoms of a residue and compared to the atomic fluctuations (Eq. 1) exhibited by the predicted structures.

### *Hinge rotations*

Hinge-bending movements of rigid domains about flexible joints are the dominating type of conformational changes documented in the Brookhaven protein data bank (Gerstein et al., 1994). Hinge-bending is also believed to allow an induced fit of molecular surfaces in protein assembly and ligand docking (Sandak et al., 1996). We examined the movements of kinesin's structural domains that can be considered to undergo rigid body motions relative to a bound microtubule with the *Hingefind* algorithm (Wriggers and Schulten, 1997a). This method identifies and visualizes effective rotation axes (hinges) of the relative movement of such domains. The identification of a hinge axis and the corresponding rotation angle provides a reduced representation of the complex movements exhibited by kinesin.

## RESULTS

### Kinesin's enzymatic site

To prepare kinesin's structure for the investigation of nucleotide-dependent changes, the ATP γ-phosphate was placed into the crystal structure of ADP-kinesin as described in Methods. Fig. 5 presents the position of the γ-phosphate in structure CT. The phosphate is found to be close to Ser-202 in kinesin's switch I region and to Gly-234 in the switch II region, consistent with the suggestion that these residues form a γ-phosphate sensor (Kull et al., 1996; Vale, 1996). A comparison of the ATP-structures ST, AT, BT, CT and DT (Table 1) revealed that a constraint of strength 5.0 kcal $mol^{-1}$ $Å^{-2}$ was necessary to induce a contact between Gly-234 and the γ-phosphate, due to the presence of slowly diffusing water molecules in the exposed enzymatic pocket. The constraint on Gly-234 also resulted in a close contact of the γ-phosphate with the switch I loop at Ser-202, i.e., the latter contact did not result from a respective constraint.

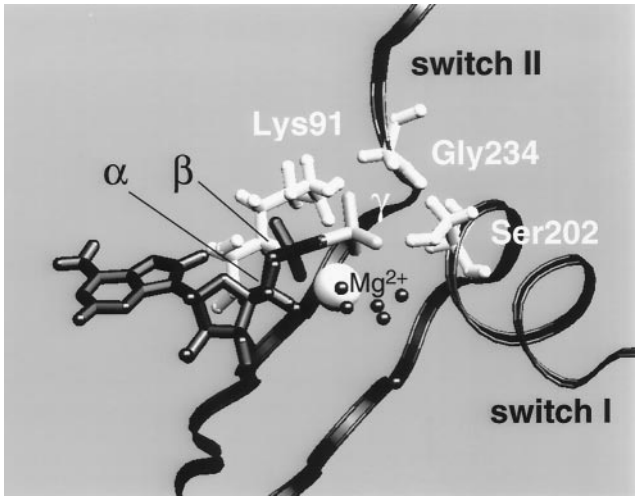


FIGURE 5 Position of the γ-phosphate in the structure CT (Table 1). ADP is shown in black licorice style, the γ-phosphate is rendered white. Also shown are the nucleotide-associated $Mg^{2+}$ ion (white van der Waals sphere) and three residues that coordinate the γ-phosphate. Water oxygens within 5 Å of the phosphate are indicated by black spheres. The figure was generated with the molecular graphics program *VMD* (Humphrey et al., 1996).

Hydrolysis of ATP occurs by attack of a water molecule on the γ-phosphate (Fersht, 1985). One expects an in-line mechanism of hydrolysis, in which the nucleophilic water approaches the γ-phosphorus from the side opposite to the $O_\beta$–$P_\gamma$ bond (Knowles, 1980). In the structures of ATP-kinesin that emerged from this study one cannot identify with certainty any water molecule that is in a position to attack the phosphorus. Several water molecules that could be poised for the attack are found within 3–5 Å of the γ-phosphate (Fig. 5). The rate of cleavage of the $O_\beta$–$P_\gamma$ bond is slow for solvated kinesin (9 $s^{-1}$), but is increased ~10-fold by binding of kinesin to a microtubule (Ma and Taylor, 1995a, b), suggesting that functional groups that depend on the conformation of the microtubule-binding site could be activating the attacking water molecule or the γ-phosphate, or both. An activation mechanism involving the serine corresponding to kinesin's Ser-202 was proposed for myosin (Fisher et al., 1995). In this model, the serine first prepares the water molecule by constraining its position relative to the γ-phosphate and then acts as an intermediary in the proton transfer from the hydrolytic water to the phosphate.

We can identify Lys-91 as a catalytic base that coordinates both the β- and the γ-phosphate with its positively charged amino group (Fig. 5). The β-γ-coordinated lysine, which is also found in G-proteins (Pai et al., 1989; Berchtold et al., 1993; Noel et al., 1993), could serve, along with $Mg^{2+}$, to stabilize the negative charge developed on the pentacoordinated γ-phosphorus in the transition state of the hydrolysis, thereby leading to enhanced catalysis.

A rendering of the molecular surface of kinesin's catalytic site (Fig. 6) reveals that ATP is bound in a sunken pocket. The mentioned catalytic Lys-91 is buried underneath the γ-phosphate. The enzymatic pocket has a solvated extension at the γ-phosphate site which could provide an attacking water molecule for the hydrolysis reaction. A simulation of phosphate release from the ATPase actin (Wriggers and Schulten, manuscript in preparation) indicated that the cleaved phosphate rotates about the attached divalent cation by 70° due to electrostatic repulsion from the β-phosphate prior to dissociation from the ion. A movement of phosphate by 3.4 Å after cleavage was also observed in crystal structures of the ATPase fragment of the bovine 70-kDa heat shock cognate protein (Flaherty et al., 1994). The solvated extension of kinesin's enzymatic pocket (Fig. 6) is large enough to accommodate such movements of the phosphate.

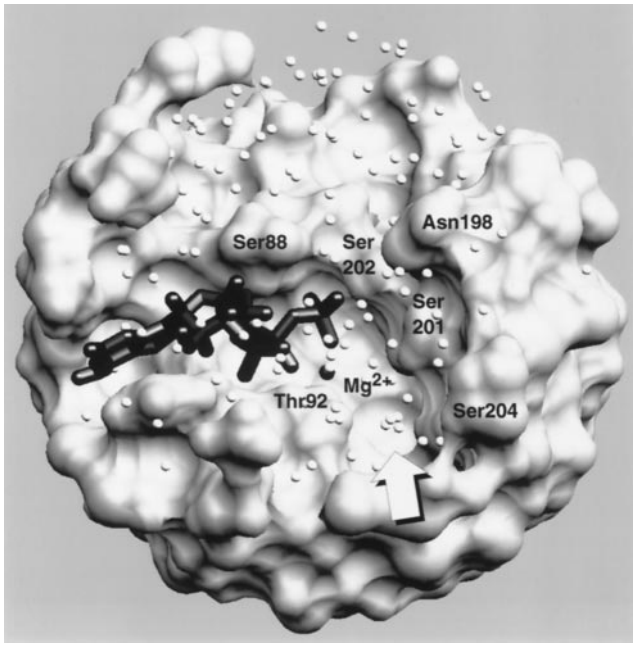


FIGURE 6 Topography of kinesin's ATP-binding site. A spherical excision of radius 15 Å centered at the γ-phosphorus reveals the surface relief of structure CT (Table 1) in the vicinity of the nucleotide (*black licorice* representation). Water oxygens within 15 Å of the γ-phosphorus are shown as white spheres. Amino acid residues on the rim of the indented nucleotide-binding site are indicated. The arrow points to an extension of the enzymatic pocket filled with water. The figure was generated with the molecular graphics program *VMD* (Humphrey et al., 1996).

## Conformational variability

It is instructive to characterize the conformational diversity exhibited by the structures before we discuss in detail kinesin's nucleotide-dependent conformational changes. The various resulting structures (Table 1) can be considered to form an ensemble representing the flexibility of the protein under the respective conformational perturbations. In Fig. 7 we compare the spatial variability exhibited by the 10 nucleotide-bound structures (Eq. 1) with spatiotemporal disorder exhibited by kinesin in the crystal calculated from crystallographic *B*-factors (Eq. 2). In the crystal, residues 1–7, 325, and 326 were too mobile for *B* factors to be observed. Of the remaining 317 residues, 49% exhibited fluctuations exceeding the crystal mobility by >30%. A small (3%) fraction of the residues showed fluctuations that were smaller by at least 30%. About half (48%) of the residues exhibited fluctuations within 30% of the crystal values. The fluctuations from the crystal *B*-factors appear to form a lower bound for the differences between the predicted structures (Fig. 7). The agreement of the observed and calculated fluctuations was better for the relatively rigid (~1 Å mobility) residues of kinesin's β-sheet core region, e.g., residues 9–14, 79–87, 206–210, 227–234, and 296–302, whereas several flexible, exposed structure elements exhibited high mobility (3–4 Å). These flexible elements include the solvent exposed loop L1 and helix α1 (Fig. 1); the exposed loop L5 (Fig. 2), which is variable between kinesin and ncd crystal structures (Sablin et al., 1996); the α2 and L10 tip of kinesin's arrowhead-shaped structure (Fig. 1); the variable helix α3 (Fig. 1); and the microtubule-binding regions L8, L11, L12, and α6 (Fig. 2).

Fig. 8 illustrates the conformational flexibility of kinesin. There is considerable movement in the tip of the structure, which is believed to form an interface with the second head in the dimer of ncd (Sosa et al., 1997). The orientation of loop L10 differs by as much as 15° between the various structures. The conformation of loop L11, which is believed to form a microtubule-binding plug (Sosa et al., 1997), appears to be very disordered. Atomic positions in this loop differ by as much as 5 Å. This flexibility of loop L11 comes as no surprise, since its tip (residues 238–254) was not part

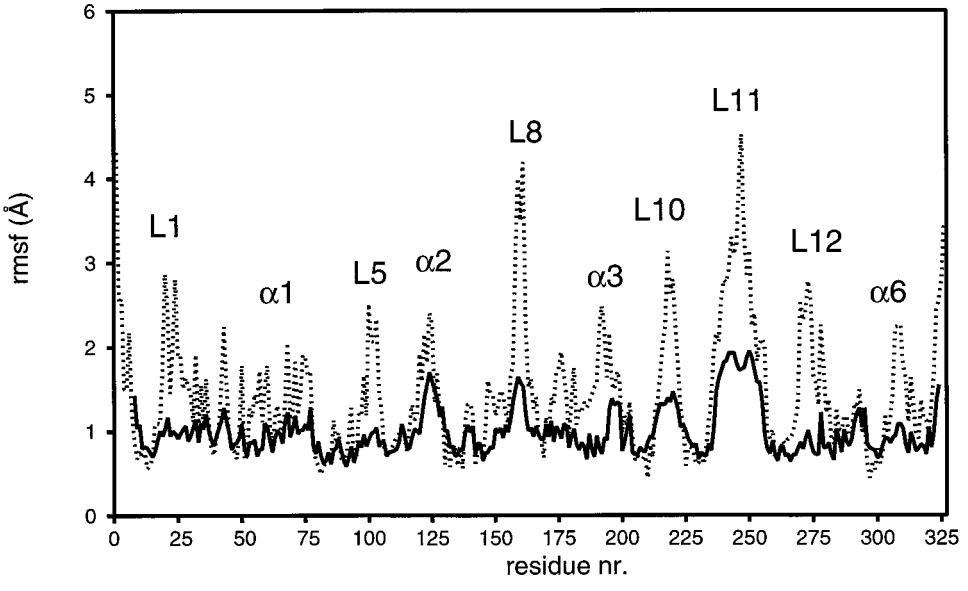


FIGURE 7 Fluctuations (Eq. 1) exhibited by the resulting nucleotide-bound kinesin structures (*dotted lines*), and fluctuations calculated from crystal *B* factors (Eq. 2; *solid lines*). For the regions of high flexibility, structure elements (Kull et al., 1996) are indicated.

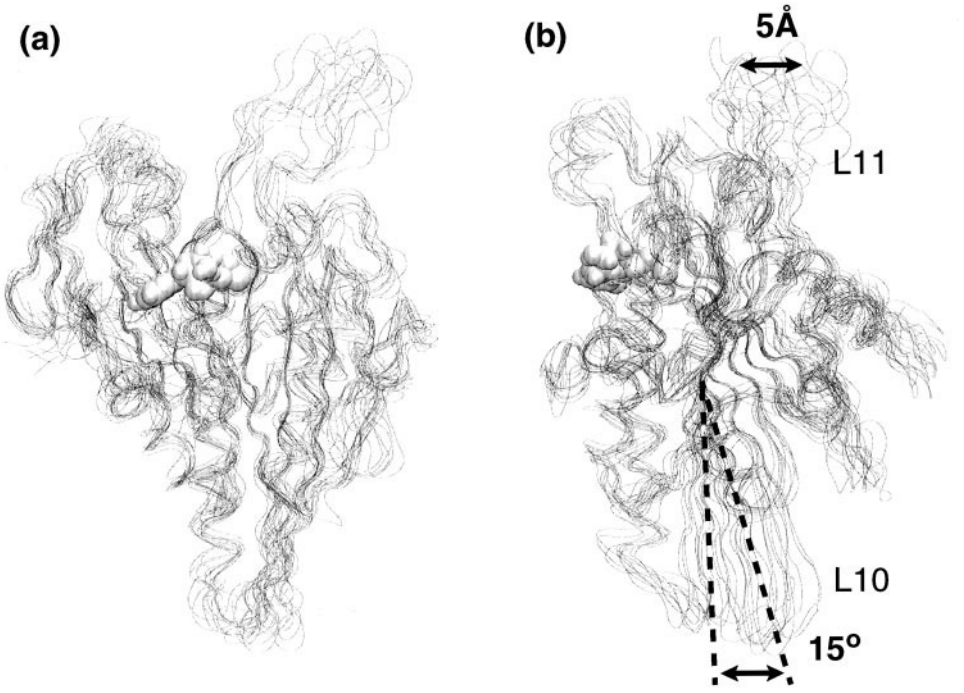


FIGURE 8 Ensemble of 10 nucleotide-bound kinesin structures, superimposed by 35 residues of kinesin's rigid $\beta$-sheet core (residues 9–14, 79–87, 206–210, 227–234, 296–302). (*a*) Front view. (*b*) Side view. The protein orientations are in accord with Figs. 1 and 2. The protein structures are represented by backbone traces. One $Mg^{2+}$-ADP nucleotide (van der Waals representation) is shown. The figure was generated with the molecular graphics program *VMD* (Humphrey et al., 1996).

of the reported kinesin structure (Kull et al., 1996) due to disorder in the crystal.

The deviation of the calculated data from the crystal fluctuation data (Fig. 7) is not unexpected and may arise for several reasons. First, the simulated annealing approach, involving temperatures of up to 500 K, increases the sampling of conformational space compared to fluctuations at room temperature. Second, the absence of crystal packing constraints in the model systems gives the exposed regions, indicated in Fig. 7, more motional freedom. Crystal constraints sometimes quench the mobility of exposed regions or even induce conformational changes in a protein, as exemplified by mobile regions in the NMR solution structure of the kinesin-related p21 ras G-protein (Kraulis et al., 1994), which exhibits significant deviations from corresponding, well-defined regions in the crystal structure (Milburn et al., 1990). Third, any nucleotide-dependent movements in the systems may contribute to the exhibited conformational diversity. A comparison of fluctuations derived from samples composed of structures with like nucleotides (Fig. 9) reveals that the enhanced fluctuations of loop L8 and helix $\alpha$3 can be attributed to differences arising from the replacement of ADP by ATP. The fluctuations shown in Fig. 9 indicate a lower mobility (3 Å) of the tip of loop L8 in contrast to the high fluctuations of 4.5 Å observed in the full set of structures (Fig. 7). Similarly, the mobility of helix $\alpha$3 is reduced to values below 1.5 Å in either ADP-kinesin or ATP-kinesin. Lower fluctuations are also observed for helix $\alpha$6 (Fig. 9, *a* and *b*) and the loops L5, L11, and L12 of the ATP-bound structures (Fig. 9 *b*). Other variable regions shown in Fig. 9 exhibit fluctuations close to those observed in the full set of structures (L1, $\alpha$1, $\alpha$2, L10), suggesting that these movements are independent of the bound nucleotide.

Structure elements that exhibit nucleotide-dependent flexibility correspond to kinesin's microtubule binding regions (Fig. 2). In the following sections we will discuss how the conformation of these elements is correlated with the type of bound nucleotide.

### The salt bridge Glu-96–Arg-190

To test the hypothesis that residues Glu-96 and Arg-190 form a salt bridge at neutral pH and that this salt bridge may be involved in nucleotide-dependent conformational changes, we simulated ADP- and ATP-kinesin in the presence and absence of the Glu-96–Arg-190 distance constraint (Fig. 10). In ADP-kinesin, the structures showed a propensity to decrease the distance between Glu-96 and Arg-190. The orientation of helix $\alpha$3 and the conformation of loop L9 appeared to be insensitive to the imposed constraint, and the salt bridge Glu-96–Arg-190 formed readily when the two residues were pulled within hydrogen-bonding distance of each other. Our results suggest that, on one hand, in ADP-kinesin Glu-96 and Arg-190 form a salt bridge at neutral pH similar to that found in ncd (Fig. 1). On the other hand, in unconstrained ATP-kinesin, the distance between Glu-96 and Arg-190 increased and helix $\alpha$3 rotated by 18° away from the nucleotide, relative to its orientation in ADP-kinesin. When Arg-190 was pulled toward Glu-96, a kink developed in helix $\alpha$3 that was accompanied by a movement of loop L9 toward the nucleotide. The movement of Arg-190 did not stabilize the desired salt bridge with Glu-96. Instead, the movement induced a salt bridge between Arg-190 and Asp-231 (Fig. 10).

The rotation of helix $\alpha$3 (residues 176–189) by far exceeds angular fluctuations originating from disorder in the

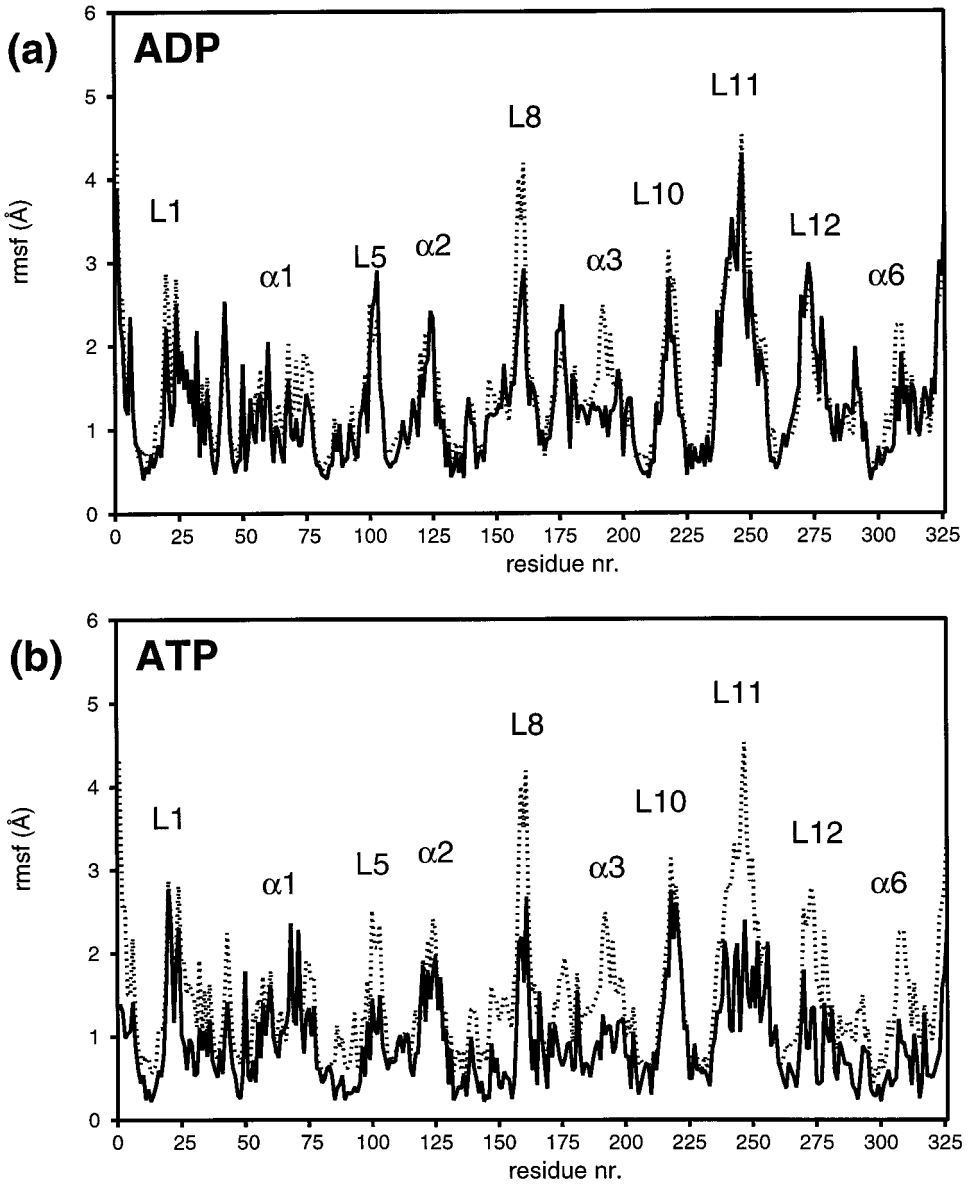


FIGURE 9 Nucleotide-dependent conformational variability. (*a*) Fluctuations (Eq. 1) exhibited by the ADP-bound kinesin structures SD, AD, BD, CD, and DD (Table 1); and (*b*) fluctuations exhibited by the ATP-bound structures AT, BT, and CT are compared to fluctuations computed for the complete set of nucleotide-bound structures (*dotted lines*). The structure ST was omitted from the set of ATP-bound structures because of the absence of the γ-phosphate–Gly-234 contact (see text). The structure DT was omitted from the set of ATP-bound structures because of an artifactual distortion of the structure in the presence of the Glu-96–Arg-190 distance constraint (see text).

structures. The helix (length 18 Å) exhibits fluctuations of 1.8 Å at its N-terminal end and fluctuations of 1.2 Å at its C-terminal end (Fig. 9). It can be shown (see Appendix, Eq. 12) that this movement corresponds to an angular fluctuation of only 2.8°, which is small compared to the observed rotation angle of 18°.

An inspection of the structures revealed that the differences in the behavior of ATP-kinesin in the presence and absence of the Glu-96–Arg-190 distance constraint may originate from changes in a second salt bridge, Glu-199–Arg-203, which is located near the γ-phosphate. In unconstrained ATP-kinesin (structures BT and CT) the contact of Ser-202 with the γ-phosphate forced Arg-203 to break from Glu-199, which resulted in a shift of loop L9 (residues 190–197) away from the nucleotide (Fig. 10 *b*). In the constrained structure DT, however, the salt bridge Glu-199–Arg-203 remained stable, as observed in the ADP-bound crystal structure. A break-up of the charge pair Glu-199–Arg-203 was predicted in the report of kinesin's crystal structure (Fig. 3 *b* in Kull et al., 1996). The authors suggested that in ATP-kinesin Arg-203 may form a new salt bridge with Glu-236. Indeed, in the structures BT and CT we observed that Arg-203 moved toward Glu-236 by 3 Å, reducing their separation to about half the value observed in

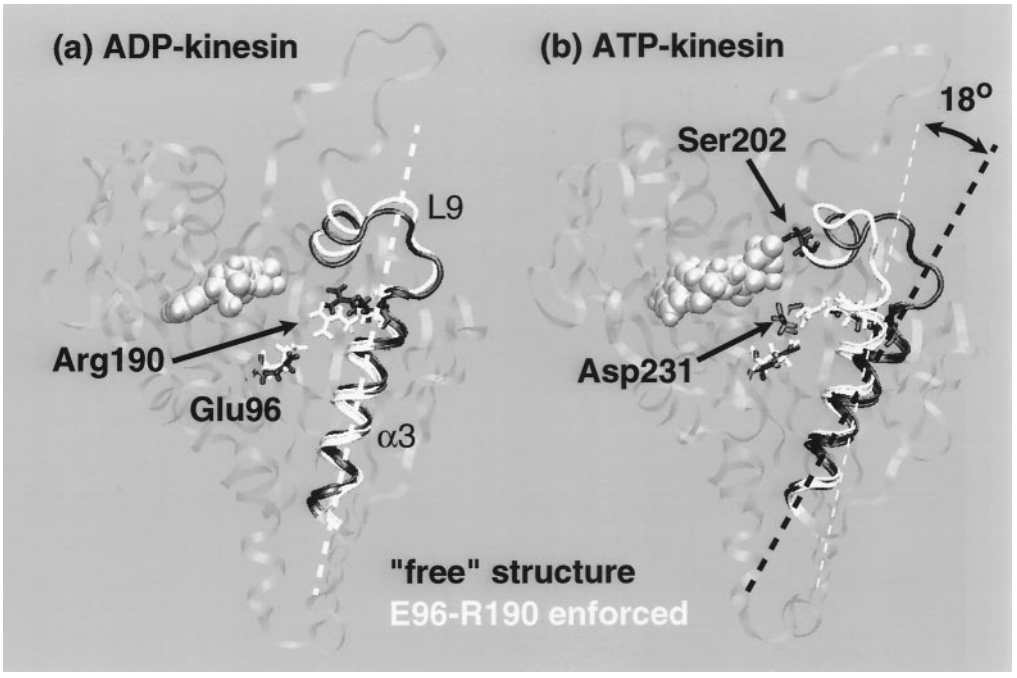


FIGURE 10 Observed orientations of helix $\alpha 3$. Emphasized are the positions of loop L9 (*tube*), helix $\alpha 3$ (*ribbon*), and individual residues of interest (*licorice*). The $Mg^{2+}$-bound nucleotide is shown in gray van der Waals representation. Structures corresponding to unconstrained Glu-96 and Arg-190 are shown in black, those corresponding to a distance constraint Glu-96–Arg-190 of strength 5.0 kcal $mol^{-1}$ $Å^{-2}$ are shown in white. (*a*) Comparison of free ADP-kinesin represented by an average of structures SD, AD, and CD (*black*) with constrained ADP-kinesin represented by an average of structures BD and DD (*white*). (*b*) Comparison of free ATP-kinesin represented by an average of structures BT and CT (*black*) with constrained ATP-kinesin represented by structure DT (*white*). The figure was generated with the molecular graphics program *VMD* (Humphrey et al., 1996).

the ADP-bound crystal structure. Two of the three unconstrained ADP-kinesin structures (AD and CD) also exhibited a break-up of the charge pair Glu-199–Arg-203 and a stronger interaction Arg-203–Glu-236, whereas in the ADP-kinesin structures BD and DD, the salt bridge Glu-199–Arg-203 was stable in the presence of the Glu-96–Arg-190 distance constraint. Our results indicate that the break-up of the salt bridge Glu-199–Arg-203 is correlated with the formation of a Glu-96–Arg-190 salt bridge.

## Allosteric effects in kinesin

It is an intriguing question how conformational changes in kinesin's nucleotide binding site can be amplified and transmitted to the microtubule-binding site. The rigidity of kinesin's $\beta$-sheet core region suggests that changes are propagated on the exposed surface of the protein, as exemplified by the rotation of helix $\alpha 3$ (Fig. 10). To identify other nucleotide-dependent movements, we superimposed ADP-kinesin (represented by an average of the structures BD and DD) and ATP-kinesin (represented by an average of the structures BT and CT) by their $\beta$-sheet core region (Fig. 11). For the illustration, kinesin's $\gamma$-phosphate sensing movements were separated into movements that can be attributed to either the switch I or the switch II $\gamma$-phosphate contact. The changes triggered by switch I involve a movement of loop L7 by 2 Å toward the nucleotide and a shift of loop L9 by 2 Å away from the nucleotide. This movement facilitated the described rotation of helix $\alpha 3$ by 18° and the break-up of salt bridge Glu-96–Arg-190 (Fig. 10). These changes are relayed to the microtubule-binding face through a shift of residues in kinesin's L8/$\beta 5$ region by 4–5 Å (Fig. 11 *a*). This nucleotide-dependent movement is large compared to the spatial disorder of 1–3 Å observed for residues 149–163 (Fig. 9).

Conformational changes induced by switch II are best understood in G-proteins (Vale, 1996). In the presence of GTP, movements of the glycine corresponding to kinesin's Gly-234 change the angle or partially melt portions of the subsequent helix (Berchtold et al., 1993; Lambright et al., 1994; Milburn et al., 1990; Mixon et al., 1995). In kinesin, the contact of the $\gamma$-phosphate with Gly-234 pulls the base of the microtubule-binding loop L11 by 2 Å toward the nucleotide (Fig. 11 *b*). This movement induces a rotation of the microtubule-binding helix $\alpha 4$ by 10° and a shift of the microtubule-binding loop L12 by 3 Å. Nucleotide-dependent movements of the microtubule-binding helices $\alpha 5$ and $\alpha 6$ (not shown) are predicted to be small. While the movement of loop L12 is of the same magnitude as the observed disorder of 3 Å (Fig. 9), the rotation of helix $\alpha 4$ (residues 256–270) is large compared to angular disorder. The helix (length 23 Å) exhibits fluctuations of 1.5 Å at both ends (Fig. 9). As discussed in the Appendix (Eq. 12), this mobility corresponds to an angular fluctuation of 2.2°, which is small compared to the observed rotation angle (10°).

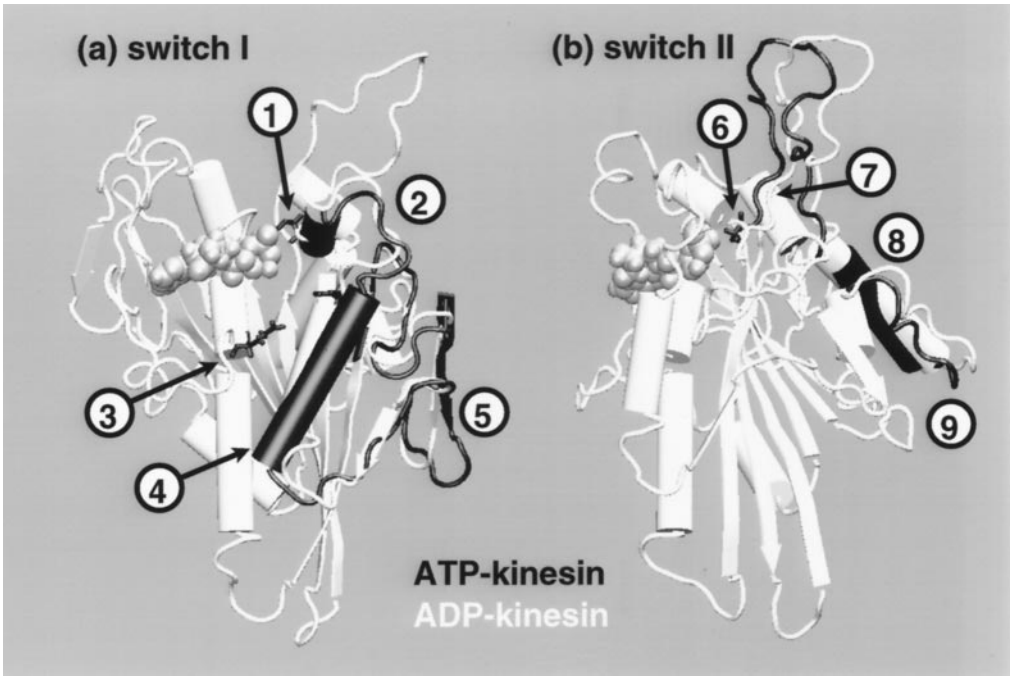


FIGURE 11 Allosteric interaction between kinesin's nucleotide- and microtubule-binding sites. The protein structures (cartoon representation) are superimposed by 35 residues of kinesin's rigid $\beta$-sheet core (residues 9–14, 79–87, 206–210, 227–234, 296–302). The $Mg^{2+}$-bound nucleotide (van der Waals representation) and certain residues of interest (licorice representation) are also shown. ADP-kinesin is represented by an average of structures BD and DD (*white*). ATP-kinesin, represented by an average of structures BT and CT (*black*), is rendered in the regions of interest. (*a*) Switch I-triggered changes (front view). Five conformational changes are indicated: (1) the contact of Ser-202 with the $\gamma$-phosphate and a rotation of helix $\alpha$3a; (2) a shift of loops L9 and L7 by 2 Å; (3) the break-up of salt bridge Glu-96–Arg-190; (4) the rotation of helix $\alpha$3 by 18°; (5) a shift of the L8/$\beta$5 microtubule-binding region by 3–5 Å. (*b*) Switch II-triggered changes (side view). Four conformational changes are indicated: (6) the contact of Gly-234 with the $\gamma$-phosphate; (7) a shift of the basis of loop L11 by 2 Å toward the nucleotide; (8) a rotation of helix $\alpha$4 by 10°; (9) a shift of loop L12 by 3 Å. The figure was generated with the molecular graphics program *VMD* (Humphrey et al., 1996).

## Microtubule interactions

The emerging model of the kinesin-microtubule complex (Sosa et al., 1997; Woehlke et al., 1997) made it possible to characterize the direction relative to the microtubule and the magnitude of the nucleotide-dependent movements of kinesin predicted in this work. Nucleotide-dependent changes control the conformation of four of kinesin's $\beta$-tubulin binding regions (L8, L11, $\alpha$4, L12), which were found by cryoelectron microscopy to form the major interaction between the motor domain and the protofilament (Sosa et al., 1997). [An animation of kinesin's nucleotide-dependent conformational changes is provided at URL ftp://ftp.ks.uiuc.edu/pub/projects/kinesin/movie.html.] These regions overlap with the binding-interface identified in mutagenesis studies, which involves primarily the structure elements L7/L8, L11, and L12/$\alpha$5 (Woehlke et al., 1997). To illustrate the effect of the bound nucleotide on the interaction with a microtubule, we superimposed in Fig. 12 the model structures of ADP- and ATP-kinesin with the L7/L8 and L12/$\alpha$5 binding regions, as identified by Woehlke et al., 1997, and aligned the protein to the microtubule surface as described by Sosa et al., 1997. We excluded loop L11 from the atom subset chosen for superposition, because L11 was found to be very flexible (Fig. 8) and it was not defined by the crystallographic data (Kull et al., 1996).

Fig. 12 illustrates that the nucleotide-dependent conformational change corresponds to a rotation of kinesin relative to the microtubule when superimposed by the regions L7/L8 and L12/$\alpha$5. In the presence of ATP, the shape of kinesin's microtubule-binding face complements the shape of the microtubule surface and brings the $\beta$-tubulin binding helix $\alpha$4 and the $\alpha$-tubulin binding helix $\alpha$6 in close proximity to the microtubule. The movement also allows loop L11 to project further into the groove between two microtubule protofilaments. In the presence of ADP, the microtubule-binding face acquires a more convex shape, which appears to weaken the protein-microtubule interactions. The position of the hinge-axis, determined by *Hingefind* (Wriggers and Schulten, 1997a), at the microtubule surface is intriguing, since it suggests a rotation of the protein about a flexible joint between kinesin and the microtubule close to the high affinity region L12/$\alpha$5. Relative to ADP-kinesin, this movement would rotate ATP-kinesin by 6.7° in the direction of the microtubule minus end.

Our choice of superimposing the structures by the regions L7/L8 and L12/$\alpha$5 was based on the results of Woehlke et al., 1997. It is possible to superimpose the structures by other combinations of putative binding regions determined by cryoelectron microscopy (Sosa et al., 1997). For example, we superimposed the model structures of ADP- and

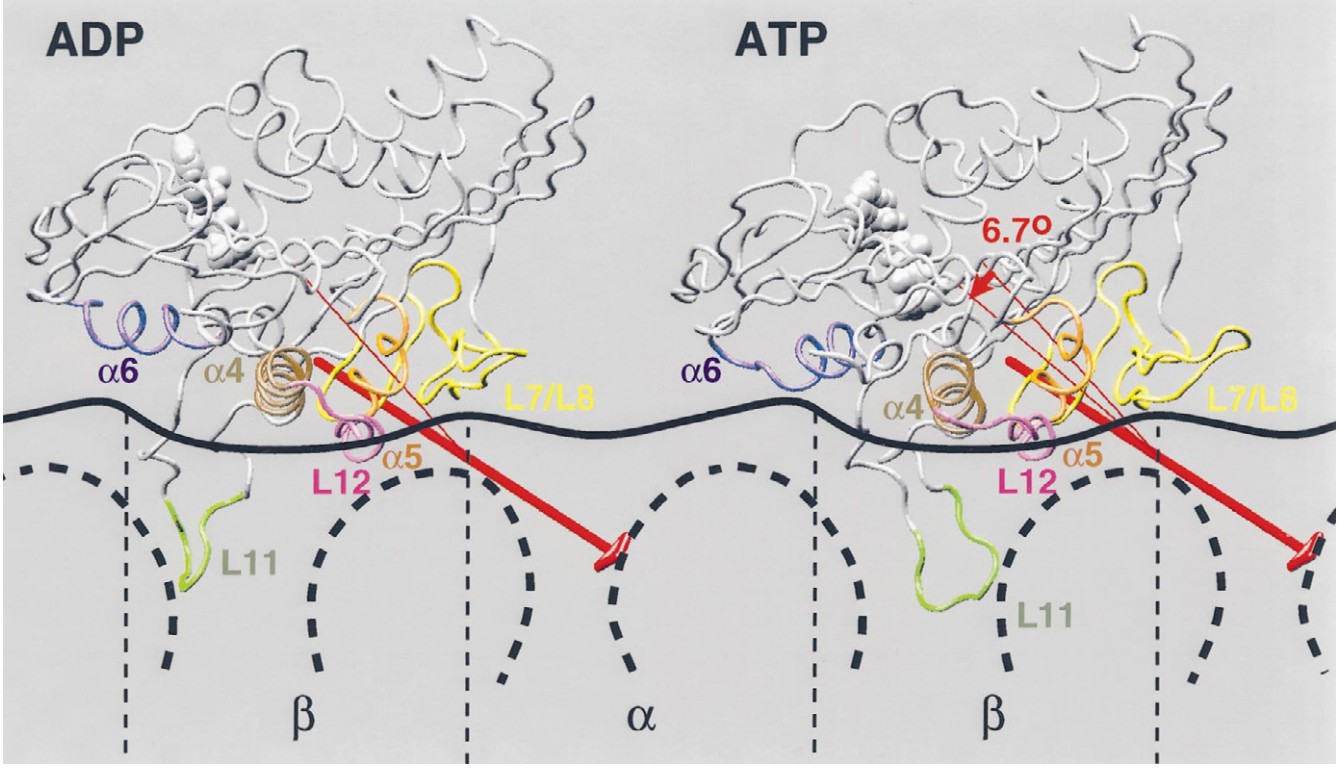


FIGURE 12 Model of nucleotide-dependent changes in kinesin's microtubule-binding interface. ADP-kinesin is represented by an average of structures BD and DD. ATP-kinesin is represented by an average of structures BT and CT. The protein is shown in tube representation, the nucleotide is shown in van der Waals representation. The structures are superimposed by the microtubule-binding regions L7/L8 (137–167, yellow), L12 (271–280, purple), and $\alpha$5 (281–290, orange), as identified by Woehlke et al., 1997. Other microtubule-binding regions, as identified by Sosa et al., 1997, are helix $\alpha$4 (256–270, brown), the tip of loop L11 (243–250, green), and helix $\alpha$6 (306–321, blue). The view is identical with Fig. 4 *a* in Sosa et al., 1997. The microtubule-protofilament surface is shown as a solid line, the surface corresponding to the grove between two microtubule-protofilaments as a dotted line (Sosa et al., 1997). The microtubule plus-end is at the right. An arrow (*red*) represents the hinge-axis about which the protein rotates in this model. The figure was generated with the molecular graphics program *VMD* (Humphrey et al., 1996).

ATP-kinesin also by their L12, $\alpha$4, and $\alpha$6 binding regions. The alignment to the microtubule track of the structures, superimposed such, resulted in a loss of contact of loop L8 in ADP-kinesin; also, the ATP-bound protein rotated by 5.2° in the direction of the microtubule plus-end relative to ADP-kinesin (not shown). The latter result implies that the direction of the nucleotide-dependent rotation of the kinesin head relative to the microtubule could be determined by the relative binding affinities of the microtubule binding regions, which may differ among the various members of the kinesin superfamily (Barton and Goldstein, 1996; Hirokawa, 1996).

The observed amplitudes of the nucleotide-dependent rotation of kinesin relative to the microtubule are larger than one would expect from thermal disorder in the structures. An analysis of rms fluctuations derived from structures bound to like-nucleotide (Fig. 9) indicates that kinesin's microtubule binding regions L7/L8, L12, and $\alpha$6 undergo fluctuations of 2.9 Å, 2.8 Å, and 2.0 Å, respectively. These fluctuations correspond (Appendix, Eq. 12) to the following rms fluctuations $\sigma_\alpha$ of the angular orientation between ATP-kinesin (average of structures BT and CT) and ADP-kinesin (average of structures BD and DD): $\sigma_\alpha = 3.8°$, when the structures are superimposed by regions L7/L8 and L12/$\alpha$5 (interface of width 25 Å, enclosed by L7/L8 and L12), and $\sigma_\alpha = 2.3°$, when the structures are superimposed by regions L12, $\alpha$4, and $\alpha$6 (interface of width 35 Å, enclosed by L12 and $\alpha$6). Compared with the actual rotations of 6.7° and 5.2°, the small fluctuations in the orientation of the protein indicate that the observed change in the shape of kinesin's microtubule-binding face is most likely a consequence of the described allosteric effect rather than due to disorder in the structures.

## DISCUSSION

By using simulated annealing, we identified conformational changes in kinesin's nucleotide binding site that are induced by the exchange of ADP by ATP. We demonstrated nucleotide-dependent allosteric effects and determined structural changes in kinesin that can be attributed to force-producing ATP hydrolysis. Our modeling effort relied on the assumption that one can arrive at structures closely resembling solvated ADP- and ATP-kinesin at neutral pH by means of few perturbations applied to the crystal structure of ADP-

kinesin (Kull et al., 1996). The applied perturbations included the addition of the ATP γ-phosphate as well as distance constraints that were based on various observations. Our model did not account for the effect of bound microtubules on the protein conformation. Microtubules induce conformational changes in kinesin that accelerate ATP hydrolysis 10-fold (Ma and Taylor, 1995a, b) and nucleotide exchange more than 1000-fold (Hackney, 1988). Despite the neglect of microtubule-induced effects, the agreement of our results with structural and biochemical evidence, as outlined in the following, suggests their validity.

The trigger for nucleotide-specific conformational changes in kinesin resides in the immediate vicinity of the γ-phosphate. As predicted earlier (Vale, 1996), kinesin's residues Gly-234 and Ser-202, which are equivalent to residues Gly-466 and Ser-243 in chicken myosin (Rayment et al., 1993) and to glycine and threonine residues in G-proteins (Vale, 1996), are involved in the sensing of the phosphate. The second serine in the γ-phosphate vicinity, Ser-201, which could compete with Ser-202 for coordination of the phosphate, did not make such contact. Mutagenesis experiments demonstrate that S202A mutants are inactive, whereas S201A kinesin still exhibits movement in motility assays, although reduced 10-fold, compared to wild-type kinesin (R. D. Vale, personal communication). The experiments thus appear to favor Ser-202 over Ser-201 as the potentially γ-phosphate-sensing amino acid in the switch I loop, consistent with our results.

The switch I contact at Ser-202 relays conformational changes to the regions L7, L8, L9, and α3. The predicted structures suggest that at neutral pH a salt bridge Glu-96–Arg-190 forms in the presence of ADP and breaks in the presence of ATP. The rotation of helix α3 by 18° (Fig. 10), which appears to be stabilized by this charge pair, is similar to the difference in orientation by 20° when ncd and kinesin structures are compared (Fig. 1 *b*).

The switch II contact at Gly-234 provides a second conformational link between kinesin's microtubule-binding face and the nucleotide. Gly-234 serves as an anchor for the microtubule-binding regions L11, α4, and L12: when in contact with the γ-phosphate of ATP-kinesin, the residue pulls loop L11 closer to the nucleotide relative to ADP-kinesin which, in turn, relays conformational changes to helix α4 and loop L12. A similar mechanism of switch II-triggered nucleotide-dependent changes was reported for myosin; according to this mechanism elements corresponding to kinesin's L11 and α4 are displaced in response to movement of a glycine (equivalent to kinesin Gly-234) toward the $A1F_4$ in an ADP-$A1F_4$ crystal structure (Fisher et al., 1995).

Kinesin's affinity for binding to the microtubule track changes during the hydrolysis cycle. In the presence of ATP and in nucleotide-free kinesin, the interaction with the microtubule is strong, and in the presence of ADP, the binding affinity is low (Romberg and Vale, 1993; Brady, 1985; Block et al., 1990; Crevel et al., 1996; Rosenfeld et al., 1996a). The simulation results presented in this work are consistent with the physical and biochemical evidence. We demonstrated that the nucleotide acts as an allosteric modifier of kinesin's microtubule-binding face. Specifically, our results suggest that the central section of ADP-kinesin's microtubule binding face bulges toward the microtubule after the loss of γ-phosphate. The conformational change would disrupt the putative contact formed by helices α4 and α6 assuming that ADP-kinesin binds exclusively to β-tubulin (Woehlke et al., 1997). The hydrolysis of ATP would correspond to a rotation of kinesin by 7° toward the plus-end of the microtubule.

The magnitude and direction of the predicted rotation of kinesin differs from the findings of Hirose et al., 1995. These authors observed by electron microscopy at 35 Å resolution a change of appearance of kinesin-decorated microtubules that was interpreted as an angular change of ATP-kinesin by 45° relative to ADP-kinesin toward the microtubule plus-end. However, the result of Hirose et al. was not reproduced by different methods or at higher resolution. It is possible that a change in the mobility of kinesin from a mobile diphosphate state to a highly ordered triphosphate state (Hirose et al., 1995) led to changes in kinesin's appearance. We expect that the rapid progress in the field will soon lead to further evidence that unambiguously determines the directionality of kinesin's nucleotide-dependent movement relative to the microtubule.

Kinesin's putative working stroke of 8 nm (Svoboda et al., 1993) is too long to be caused by the conformational changes presented in this work or by any other conceivable change in a single motor domain. One hypothesis is that movement of the second, unattached head in the kinesin dimer relative to the attached head amplifies the ATP-driven conformational change (Howard, 1997). In principle, this movement could be accomplished by diffusion or by a direct conformational link between the heads (a lever arm) or by both. Kinetic studies demonstrated that kinesin's two heads move along cytoskeletal filaments in a cooperative manner, in which the binding of ATP to an attached head induces binding to the microtubule and subsequent ADP-release in the other, unattached head that is paused in the ADP-state (Schnapp et al., 1990; Gilbert et al., 1995; Berliner et al., 1995; Hackney, 1994; Ma and Taylor, 1997). This mechanism could facilitate a rotation of the monomers (Howard, 1996) in a hand-over-hand mechanism of motion (Hackney, 1994). Structural details of this interaction between the heads are unknown, although fluorescence spectroscopy measurements provided evidence of a hinge between the motor domains, whose flexibility may change during kinesin's hydrolysis cycle (Rosenfeld et al., 1996b).

The structures presented in this work exhibit significant flexibility in the tip of the arrowhead-shaped motor domain (Fig. 8 *b*); this flexible tip forms an interface to the second head in the ncd dimer (Sosa et al., 1997), consistent with the idea of a hinge between the two heads. The crystal structure of dimeric kinesin may allow one to investigate an allosteric coupling between the two motor domains. Knowledge of the dimer interface would permit an interpretation of the

effect of thermal variability and of nucleotide-dependent conformational changes on the relative orientation of the monomers. Since computer simulations of biomolecular systems of 100,000 atoms have become feasible, the tumbling motion of two kinesin heads in a solvated kinesin dimer is amenable to further modeling studies.

## APPENDIX

We seek to derive estimates of angular disorder exhibited by a three-dimensional vector $\vec{l} = \vec{x}_2 - \vec{x}_1$ in terms of the spatial disorder exhibited by its two end points $\vec{x}_i$ ($i = 1, 2$). Noise-related displacements of the end points are described by

$$\vec{x}_i = \vec{x}_{i0} + \Delta\vec{x}_i \ (i = 1, 2), \tag{3}$$

where the $\vec{x}_{i0}$ describe the average position of $\vec{x}_i$, and the displacements $\Delta\vec{x}_i$ are three-dimensional random vectors of standard deviation $\sigma_i$ ($i = 1, 2$). For averages $\langle \cdots \rangle$ in the limit of a large number of realizations of random displacements holds $\langle \Delta\vec{x}_i \rangle = 0$ and $\langle \Delta\vec{x}_i^2 \rangle = \sigma_i^2$ ($i = 1, 2$).

We are interested in fluctuations in the angular orientation exhibited by $\vec{l}$ about a perpendicular axis $\vec{r}$ (view direction). The displacements $\Delta\vec{x}_i$ can be characterized by coefficients $\Delta a_i$, $\Delta b_i$, $\Delta c_i$ in the coordinate system defined by $\vec{l}$, $\vec{r}$, and the cross product $\vec{l} \times \vec{r}$:

$$\Delta\vec{x}_i = \Delta a_i \left( \frac{\vec{l}}{|\vec{l}|} \right) + \Delta b_i \left( \frac{\vec{r}}{|\vec{r}|} \right) + \Delta c_i \left( \frac{\vec{l} \times \vec{r}}{|\vec{l} \times \vec{r}|} \right) (i = 1, 2). \tag{4}$$

The averages of $\Delta a_i$, $\Delta b_i$, $\Delta c_i$ vanish and for the variances holds

$$\langle \Delta\vec{x}_i^2 \rangle = \langle \Delta a_i^2 \rangle + \langle \Delta b_i^2 \rangle + \langle \Delta c_i^2 \rangle = \sigma_i^2 \ (i = 1, 2). \tag{5}$$

We assume isotropic random displacements, i.e.,

$$\langle \Delta a_i^2 \rangle = \langle \Delta b_i^2 \rangle = \langle \Delta c_i^2 \rangle = \frac{1}{3}\sigma_i^2 \ (i = 1, 2). \tag{6}$$

The angular change of the orientation of $\vec{l}$ as seen by the viewer, $\Delta\alpha$, is given by

$$\tan(\Delta\alpha) = \frac{\Delta c_2 - \Delta c_1}{|\vec{l}|}. \tag{7}$$

For small $\Delta\alpha$ (expressed in radian units) $\tan(\Delta\alpha) \approx \Delta\alpha$. It is straightforward to derive the standard deviation of the angular change, $\sigma_\alpha = \sqrt{\langle \Delta\alpha^2 \rangle}$, with the help of Eq. 6 in this limit of small angular changes:

$$\sigma_\alpha = \sqrt{\frac{\sigma_1^2 + \sigma_2^2}{3|\vec{l}|^2}}. \tag{8}$$

The standard deviations $\sigma_1$ and $\sigma_2$ can be identified with the rms fluctuations (Eq. 1) exhibited by the two ends of an extended protein structure segment, whose angular disorder $\sigma_\alpha$ relative to the observer we seek to estimate.

### Angular disorder estimated for two averaged sets of coordinates

In a structure derived from an average of two sets of coordinates (I and II), the variances of the random displacements in an individual set of coordinates are given by

$$\langle (\Delta\vec{x}_i^{\,\mathrm{I}})^2 \rangle = \langle (\Delta\vec{x}_i^{\,\mathrm{II}})^2 \rangle = \sigma_i^2 \ (i = 1, 2). \tag{9}$$

The observed displacements $\Delta\vec{x}_i$ (Eq. 3) average to

$$\Delta\vec{x}_i = \frac{\Delta\vec{x}_i^{\,\mathrm{I}} + \Delta\vec{x}_i^{\,\mathrm{II}}}{2} \ (i = 1, 2). \tag{10}$$

We can compute the variances of the $\Delta\vec{x}_i$ with the help of Eq. 9:

$$\langle \Delta\vec{x}_i^2 \rangle = \frac{1}{2}\sigma_i^2 \ (i = 1, 2). \tag{11}$$

The angle rms fluctuations $\sigma_\alpha$ are then

$$\sigma_\alpha = \sqrt{\frac{\sigma_1^2 + \sigma_2^2}{6|\vec{l}|^2}}. \tag{12}$$

We note that $\sigma_\alpha$ in Eqs. 8 and 12 is in radian units.

The authors thank F. Jon Kull, Robert J. Fletterick, and Ronald D. Vale for valuable discussion and for providing the crystal structures of kinesin and ncd.

This work was supported by National Institutes of Health Grant PHS 5 P41, RR05969-04, National Science Foundation Grants BIR-9318159 and BIR 94-23827 (EQ), the Roy J. Carver Charitable Trust, and Computertime Grant MCA93S028P at the Pittsburgh Supercomputing Center.

## REFERENCES

Arnal, I., F. Metoz, S. DeBonis, and R. Wade. 1996. Three-dimensional structure of functional motor proteins on microtubules. *Curr. Biol.* 6:1265–1270.

Barton, N., and L. Goldstein. 1996. Going mobile: microtubule motors and chromosome segregation. *Proc. Natl. Acad. Sci. USA,* 93:1735–1742.

Berchtold, H., L. Reshetnikova, C. O. Reiser, N. K. Schirmer, M. Sprinzl, and R. Hilgenfeld. 1993. Crystal structure of active elongation factor Tu reveals major domain rearrangements. *Nature.* 365:126–132.

Berliner, E., E. Young, K. Anderson, H. Mahtani, and J. Gelles. 1995. Failure of a single-headed kinesin to track parallel to microtubule protofilaments. *Nature.* 373:718–721.

Block, S., L. Goldstein, and B. Schnapp. 1990. Bead movement by single kinesin molecules studied with optical tweezers. *Nature.* 348:348–352.

Brady, S. 1985. A novel brain ATPase with properties expected for the fast axonal transport motor. *Nature.* 317:73–75.

Brooks, B. R., R. E. Bruccoleri, B. D. Olafson, D. J. States, S. Swaminathan, and M. Karplus. 1983. CHARMM: a program for macromolecular energy, minimization, and dynamics calculations. *J. Comp. Chem.* 4:187–217.

Brünger, A. 1991. Simulated annealing in crystallography. *Annu. Rev. Phys. Chem.* 42:197–223.

Brünger, A. T. 1992. X-PLOR, Version 3.1: A System for X-ray Crystallography and NMR. The Howard Hughes Medical Institute and Department of Molecular Biophysics and Biochemistry, Yale University, New Haven, CT.

Brünger, A. T., A. Krukowski, and J. Erickson. 1990. Slow-cooling protocols for crystallographic refinement by simulated annealing. *Acta Crystallogr.* A46:585–593.

Cantor, C. R., and P. R. Schimmel. 1980. Biophysical Chemistry, Vol. I. W. H. Freeman and Company, New York.

Collins, J. R., S. K. Burt, and J. W. Erickson. 1995. Flap opening in HIV-1 protease simulated by "activated" molecular dynamics. *Nat. Struct. Biol.* 2:334–338.

Crevel, I.-T., A. Lockhart, and R. Cross. 1996. Weak and strong states of kinesin and ncd. *J. Mol. Biol.* 257:66–76.

Daggett, V., and M. Levitt. 1993. Realistic simulations of native-protein dynamics in solution and beyond. *Annu. Rev. Biophys. Biomol. Struct.* 22:353–380.

Ernst, J., R. Clubb, H.-X. Zhou, A. Gronenborn, and G. Clore. 1995. Demonstration of positionally disordered water within a protein hydrophobic cavity by NMR. *Science.* 267:1813–1817.

Fersht, A. 1985. Enzyme Structure and Mechanism. W. H. Freeman and Co., New York.

Fisher, A., C. Smith, J. Thoden, R. Smith, K. Sutoh, H. Holden, and I. Rayment. 1995. X-ray structures of the myosin motor domain of *Dictyostelium discoideum* complexed with MgADP.$BeF_x$ and MgADP.$AlF_4^-$. *Biochemistry.* 34:8960–8972.

Flaherty, K. M., S. M. Wilbanks, C. DeLuca-Flaherty, and D. B. McKay. 1994. Structural basis of the 70-kilodalton heat shock cognate protein ATP hydrolytic activity. *J. Biol. Chem.* 269:12899–12907.

Frauenfelder, H., S. G. Sligar, and P. G. Wolynes. 1991. The energy landscapes and motions of proteins. *Science.* 254:1598–1603.

Gerstein, M., A. M. Lesk, and C. Chothia. 1994. Structural mechanisms for domain movements in proteins. *Biochemistry.* 33:6739–6749.

Gilbert, S., M. Webb, M. Brune, and K. Johnson. 1995. Pathway of processive ATP hydrolysis by kinesin. *Nature.* 373:671–676.

Guàrdia, E., and J. A. Padró. 1996. On the structure and dynamic properties of aqueous solutions: molecular dynamics simulation of $Cl^-$ and $Cl^{2-}$ in water. *Mol. Simul.* 17:83–94.

Hackney, D. 1988. Kinesin ATPase: rate-limiting ADP release. *Proc. Natl. Acad. Sci. USA.* 85:6314–6318.

Hackney, D. 1994. Evidence for alternating head catalysis by kinesin during microtubule-stimulated ATP hydrolysis. *Proc. Natl. Acad. Sci. USA.* 91:6865–6869.

Hackney, D. 1996. The kinetic cycles of myosin, kinesin, and dynein. *Annu. Rev. Physiol.* 58:731–750.

Henningsen, U., and M. Schliwa. 1997. Reversal in the direction of movement of a molecular motor. *Nature.* 389:93–95.

Hirokawa, N. 1996. Organelle transport along microtubules—the role of KIFs. *Trends Cell Biol.* 6:135–141.

Hirose, K., W. Amos, A. Lockhart, R. Cross, and L. Amos. 1997. Three-dimensional cryoelectron microscopy of 16-protofilament microtubules: structure, polarity, and interaction with motor proteins. *J. Struct. Biol.* 118:140–148.

Hirose, K., A. Lockhart, R. Cross, and L. Amos. 1996. Three-dimensional cryoelectron microscopy of dimeric kinesin and ncd motor domains on microtubules. *Proc. Natl. Acad. Sci. USA.* 93:9539–9544.

Hirose, K., A. Lockhart, R. A. Cross, and L. A. Amos. 1995. Nucleotide-dependent angular change in kinesin motor domain bound to tubulin. *Nature.* 376:277–279.

Hoenger, A., and R. Milligan. 1997. Motor domains of kinesin and ncd interact with microtubule protofilaments with the same binding geometry. *J. Mol. Biol.* 265:553–564.

Howard, J. 1996. The movement of kinesin along microtubules. *Annu. Rev. Physiol.* 58:703–729.

Howard, J. 1997. Molecular motors: structural adaptations to cellular functions. *Nature.* 389:561–567.

Howard, J., A. Hudspeth, and R. Vale. 1989. Movement of microtubules by single kinesin molecules. *Nature.* 342:154–158.

Huber, G., and J. McCammon. 1997. Weighted-ensemble simulated annealing: faster optimization on hierarchical energy surfaces. *Physiol. Rev. E.* 55:4822–4825.

Humphrey, W. F., A. Dalke, and K. Schulten. 1996. VMD—Visual molecular dynamics. *J. Mol. Graphics.* 14:33–38.

Jorgensen, W. L., J. Chandrasekhar, J. D. Madura, R. W. Impey, and M. L. Klein. 1983. Comparison of simple potential functions for simulating liquid water. *J. Chem. Phys.* 79:926–935.

Kabsch, W. 1976. A solution for the best rotation to relate two sets of vectors. *Acta Crystallogr. A.* 32:922–923.

Kabsch, W., H. Mannherz, D. Suck, E. Pai, and K. Holmes. 1990. Atomic structure of the actin:DNase I complex. *Nature.* 347:37–44.

Knowles, J. 1980. Enzyme-catalyzed phosphoryl transfer reactions. *Annu. Rev. Biochem.* 49:877–919.

Kraulis, P., P. Domaille, S. Campbell-Burk, T. Van Aken, and E. Laue. 1994. Solution structure and dynamics of ras p21.GDP determined by heteronuclear three- and four-dimensional NMR spectroscopy. *Biochemistry.* 33:3515–3531.

Kull, F. J., E. P. Sablin, R. Lau, R. J. Fletterick, and R. D. Vale. 1996. Crystal structure of the kinesin motor domain reveals a structural similarity to myosin. *Nature.* 380:550–555.

Lambright, D. G., J. P. Noel, H. E. Hamm, and P. B. Sigler. 1994. Structural determinants for activation of the $\alpha$-subunit of a heterotrimeric G-protein. *Nature.* 369:621–628.

Lockhart, A., and R. Cross. 1994. Origins of reversed directionality in the ncd molecular motor. *EMBO J.* 13:751–757.

Lockhart, A., R. Cross, and D. McKillop. 1995. ADP release is the rate-limiting step of the MT activated ATPase of non-claret disjunctional and kinesin. *FEBS Lett.* 368:531–535.

Ma, Y.-Z., and E. Taylor. 1995a. Kinetic mechanism of kinesin motor domain. *Biochemistry.* 34:13233–13241.

Ma, Y.-Z., and E. Taylor. 1995b. Mechanism of microtubule kinesin ATPase. *Biochemistry.* 34:13242–13251.

Ma, Y.-Z., and E. W. Taylor. 1997. Interacting head mechanism of microtubule-kinesin ATPase. *J. Biol. Chem.* 272:724–730.

McDonald, H., and L. Goldstein. 1990. Identification and characterization of a gene encoding a kinesin-like protein in *Drosophila. Cell.* 61: 991–1000.

McDonald, H., R. Stewart, and L. Goldstein. 1990. The kinesin-like ncd protein of *Drosophila* is a minus-end directed microtubule motor. *Cell.* 63:1159–1165.

Milburn, M. V., L. Tong, A. M. de Vos, A. Brunger, Z. Yamaizumi, S. Nishimura, and S.-H. Kim. 1990. Molecular switch for signal transduction: structural differences between active and inactive forms of protooncogenic ras proteins. *Science.* 247:939–945.

Mixon, M. B., E. Lee, D. E. Coleman, A. M. Berghuis, A. G. Gilman, and S. R. Sprang. 1995. Tertiary and quaternary structural changes in $G_{i\alpha 1}$ induced by GTP hydrolysis. *Science.* 270:954–960.

Morii, H., T. Takenawa, F. Arisaka, and T. Shimizu. 1997. Identification of kinesin neck region as a stable $\alpha$-helical coiled coil and its thermodynamic characterization. *Biochemistry.* 36:1933–1942.

Noel, J. P., H. E. Hamm, and P. B. Sigler. 1993. The 2.2 Å crystal structure of transducin complexed with GTP$\gamma$S. *Nature.* 366:654–663.

Pai, E. F., W. Kabsch, U. Krengel, K. C. Holmes, J. John, and A. Wittinghofer. 1989. Structure of the guanine-nucleotide-binding domain of the Ha-ras oncogene product p21 in the triphosphate conformation. *Nature.* 341:209–214.

Pastor, R. W. 1994. Techniques and applications of Langevin dynamics simulations. *In* The Molecular Dynamics of Liquid Crystals. G. R. Luckhurst and C. A. Veracini, editors. Kluwer, the Netherlands.

Rayment, I. 1996. Kinesin and myosin: molecular motors with similar engines. *Structure.* 4:501–504.

Rayment, I., W. R. Rypniewski, K. Schmidt-Bäse, R. Smith, D. R. Tomchick, M. M. Benning, D. A. Winkelmann, G. Wesenberg, and H. M. Holden. 1993. Three-dimensional structure of myosin subfragment-1: a molecular motor. *Science.* 261:50–58.

Romberg, L., and R. Vale. 1993. Chemomechanical cycle of kinesin differs from that of myosin. *Nature.* 361:168–170.

Rosenfeld, S., J. Correia, J. Xing, B. Rener, and H. Cheung. 1996b. Structural studies of kinesin-nucleotide intermediates. *J. Biol. Chem.* 271:30212–30221.

Rosenfeld, S., B. Rener, J. Correia, M. Mayo, and H. Cheung. 1996a. Equilibrium studies of kinesin-nucleotide intermediates. *J. Biol. Chem.* 271:9473–9482.

Sablin, E., and R. Fletterick. 1995. Crystallization and preliminary structural studies of the ncd motor domain. *Proteins Struct. Funct. Genet.* 21:68–69.

Sablin, E. P., F. J. Kull, R. Cooke, R. D. Vale, and R. J. Fletterick. 1996. Crystal structure of the motor domain of the kinesin-related motor ncd. *Nature.* 380:555–559.

Sandak, B., R. Nussinov, and H. J. Wolfson. 1996. Docking of conformationally flexible proteins. *Proceedings of the 1996 Symposium on Combinatorial Pattern Matching, Lecture Notes in Computer Science,* Vol. 1075. D. Hirshberg, and G. Myers, editors. Springer Verlag, New York.

Schnapp, B., C. Crise, M. Sheetz, T. Reese, and S. Khan. 1990. Delayed start-up of kinesin-driven microtubule gliding following inhibition by adenosine 5′-[$\beta,\gamma$-imido]triphosphate. *Proc. Natl. Acad. Sci. USA.* 87: 10053–10057.

Sellers, J. 1996. Kinesin and ncd, two structural cousins of myosin. *J. Muscle Res. Cell Motil.* 17:173–175.

Shimizu, T., E. Sablin, R. Vale, R. Fletterick, E. Pechatnikova, and E. Taylor. 1995. Expression, purification, ATPase properties, and microtubule-binding properties of the ncd motor domain. *Biochemistry.* 34: 13259–13266.

Smith, C., and I. Rayment. 1996. X-ray structure of the magnesium (II).ADP.vanadate complex of the *Dictyostelium discoideum* myosin motor domain to 1.9 Å resolution. *Biochemistry.* 35:5404–5417.

Sosa, H., P. Dias, A. Hoenger, M. Whittaker, E. Wilson-Kubalek, E. Sablin, R. Fletterick, R. Vale, and R. Milligan. 1997. A model for the microtubule-ncd motor protein complex obtained by cryo-electron microscopy and image analysis. *Cell.* 90:217–224.

Steinbach, P. J., and B. R. Brooks. 1993. Protein hydration elucidated by molecular dynamics simulation. *Proc. Natl. Acad. Sci. USA.* 90: 9135–9139.

Stewart, R., J. Thaler, and L. Goldstein. 1993. Direction of microtubule movement is an intrinsic property of the motor domain of kinesin heavy chain and *Drosophila* ncd protein. *Proc. Natl. Acad. Sci. USA.* 90: 5209–5213.

Svoboda, K., C. Schmidt, B. Schnapp, and S. Block. 1993. Direct observation of kinesin stepping by optical trapping interferometry. *Nature.* 365:721–727.

Teeter, M. M. 1991. Water-protein interactions: theory and experiment. *Annu. Rev. Biophys. Biophys. Chem.* 20:577–600.

Vale, R. D. 1996. Switches, latches, and amplifiers: common themes of G-proteins and molecular motors. *J. Cell Biol.* 135:291–302.

Vale, R., B. Schnapp, T. Mitchinson, E. Steuer, T. Reese, and M. Sheetz. 1985. Different axoplasmic proteins generate movement in opposite directions along microtubules in vitro. *Cell.* 43:623–632.

van Laarhoven, P. J. M., and E. H. L. Aarts. 1987. Simulated Annealing: Theory and Application. D. Reidel, Dordrecht, The Netherlands.

Walker, R., E. Salmon, and S. Endow. 1990. The *Drosophila claret* segregation protein is a minus-end directed motor molecule. *Nature.* 347:780–782.

Westhof, E. 1993. Water and biological macromolecules. CRC Press Inc., Boca Raton, Florida.

Woehlke, G., A. Ruby, C. Hart, B. Ly, N. Hom-Boohrer, and R. Vale. 1997. Microtubule interaction site of the kinesin motor. *Cell.* 90: 207–216.

Wriggers, W., and K. Schulten. 1997a. Protein domain movements: detection of rigid domains and visualization of hinges in comparisons of atomic coordinates. *Proteins. Struct. Funct. Genet.* 29:1–14.

Wriggers, W., and K. Schulten. 1997b. Stability and dynamics of G-actin: back door water diffusion and behavior of a subdomain 3/4 loop. *Biophys. J.* 73:624–639.

Yang, J., W. Saxton, R. Stewart, E. Raff, and L. Goldstein. 1990. Evidence that the head of kinesin is sufficient for force generation and motility in vitro. *Science.* 249:42–47.

Zhang, L., and J. Hermans. 1996. Hydrophilicity of cavities in proteins. *Proteins Struct. Funct. Genet.* 24:433–438.